J. Fluid Mech. (1987), *vol.* 180, *pp.* 147–169
Printed in Great Britain

Characteristics of turbulent flow in slightly heated free swirling jets

By J. W. ELSNER AND L. KURZAK
Thermal Machinery Institute, Technical University of Częstochowa, Deglera 35, 42–200 Częstochowa, Poland

(Received 16 December 1985 and in revised form 1 December 1986)

Slightly heated swirling jets have been investigated experimentally in order to determine the effect of swirl degree on the mean and turbulent flow pattern. In particular, it has been shown that the swirl action strongly intensifies the turbulent momentum and heat transport processes in the close vicinity of the jet outlet and tends to quench them further downstream.

1. Introduction

Free swirling jets often occur in various mechanical, power-producing and chemical devices. They are used to control flames in combustion chambers and have also been applied in different types of spray guns and burners. One of the first attempts at a theoretical description of a laminar free swirling jet was undertaken by Loytsyanskii (1953). Research on turbulent swirling jets was mainly carried out using experimental methods because of the complexity of the flow phenomena and difficulties connected with their precise analytic description. From among the works performed in this field one should mention the research of Rose (1962), Chigier & Chervinsky (1967), Achmedov (1977), Pratte & Keffer (1972), Elsner & Drobniak (1979, 1983), Grandmaison & Becker (1982) and others.

The problem of non-isothermal free swirling jets has seldom been considered in the scientific literature, but was studied, among other subjects, by Curtet & Darigol (1978) who investigated experimentally the fields of mean velocity and mean temperatures as well as the distributions of correlations $\overline{u_x u_r}$ and $\overline{u_r \vartheta}$ for various swirl degrees. A series of tests on a slightly heated swirling jet were also performed by Ogawa, Hatakayama & Fujita (1979, 1981, 1982). However, their results were related only to the evolution of mean-velocity and mean-temperature fields. Komori & Ueda (1985) dealt with the flow structure of a slightly heated swirling jet with an irrotational, low-speed, coflowing stream. However, their considerations have been restricted mainly to the close vicinity of the nozzle exit, being the region of intense mixing and large entrainment from the ambient coflowing stream towards the jet.

As may be seen from the short review above there is still a lack of complete and properly systematized data concerning the effect of swirl action on the processes of turbulent momentum and heat transfer. An attempt to determine that effect was thus undertaken in this work.

2. Test apparatus and experimental procedure

In the previous investigations a number of methods were used to generate swirl. Rose (1962), Pratte & Keffer (1972) as well as Komori & Ueda (1985) rotated a pipe

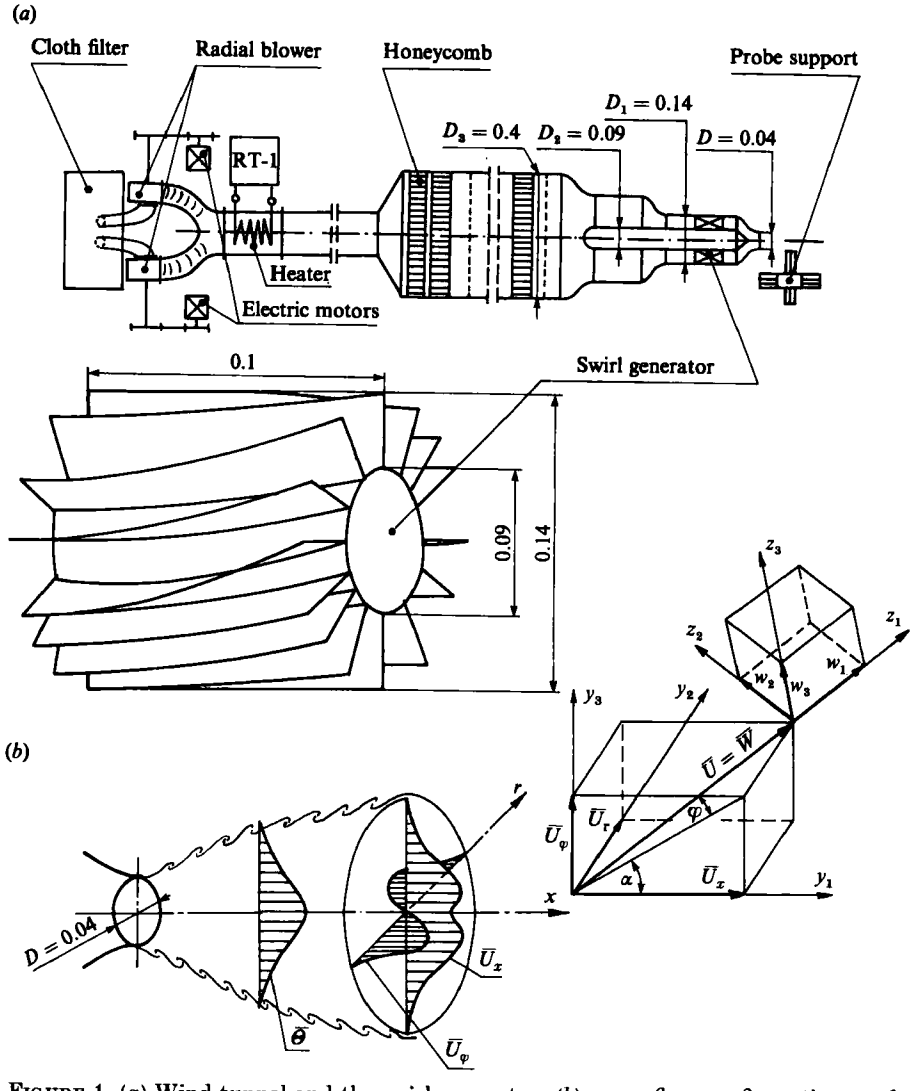

FIGURE 1. (*a*) Wind tunnel and the swirl generator; (*b*) mean-flow configurations and coordinate systems.

or a convergent nozzle at high speed. Chigier & Beér (1964) and Curtet & Darigol (1978) varied the swirl degree by changing the proportions of air introduced axially and tangentially into the swirl generator.

In our investigations, as in the experiments of Kerr & Fraser (1965) or Grandmaison & Becker (1982), the swirl was produced by means of several sets of angled vanes located in the outlet part of the wind tunnel, shown schematically in figure 1 (*a*). The geometry of the blade rings, composed of twelve suitably shaped profiles, made it possible to obtain different values of swirl degree

$$s = \frac{\int_0^\infty \rho \bar{U}_x \bar{U}_\varphi r^2 \, \mathrm{d}r}{R \int_0^\infty \rho (\bar{U}_x^2 - 0.5 \bar{U}_\varphi^2) r \, \mathrm{d}r},$$

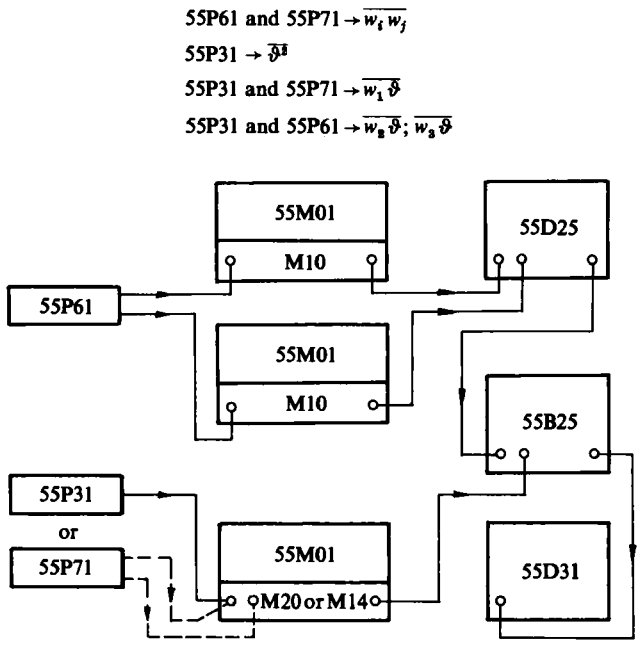

FIGURE 2. Block diagram of an experimental set-up for the measurements of turbulent quantities.

increasing up to 0.42, and defined as the ratio of axial flux of angular momentum to the axial flux of linear momentum multiplied by the outlet-nozzle radius ($R = 0.02$ m). Both of these fluxes are to be conserved along the jet axis and may therefore be evaluated from integration of velocity profiles at an arbitrary cross-section of the jet.

In order to equalize the circumferential non-homogeneity of the flow, caused by the wakes behind the trailing edges of the blades, considerable contraction of flow was applied at the tunnel exit by means of a nozzle having an outlet diameter $D = 0.04$ m. The axisymmetric character of the flow has been confirmed by the distributions of mean temperature $\overline{\Theta}$ and mean axial velocity $\overline{U}_x$ measured at the exit plane along the half-circumference located at the radius $r = 0.2D$. The results, not shown here, exhibit no trace of wakes produced by the angled vanes, so that further measurements could be performed along one radius only. The air, supplied by two radial blowers with an adjustable speed, was heated electrically to the temperature $\overline{\Theta}_{\text{ave}} = 40°$ above the ambient one. This value for all the swirling and non-swirling jets was kept constant with accuracy up to 0.2° by means of an RT-1 regulator produced by Wilher Co. The flow rate for all the swirl degrees was also maintained at a constant level, so that the Reynolds number, based on the axial mean velocity $\overline{U}_{\text{ave}} = 37.5$ m/s averaged at the nozzle exit, was $Re_D \approx 8 \times 10^4$.

The measurements of flow quantities were performed in the planes $x = \text{const.}$ perpendicular to the jet axis within the range $x/D \leqslant 15$. Mean velocity and its spatial direction, determined by the angles $\alpha(x, r)$ and $\varphi(x, r)$, were found with the help of a miniature five-hole spherical probe. Turbulence characteristics were measured in a local, streamwise-orientated Cartesian coordinate system $z_i(\overline{w} = \overline{w}_1; \overline{w}_2 = \overline{w}_3 = 0)$ with the use of three-channel DISA 55-M system hot-wire anemometer (figure 2), equipped with 55P61 X-array probes, 55P71 temperature-compensated probes and

55P31-type resistance thermometers. By rotating the X-wire probe about the z_1-axis (figure 1*b*) and combining its voltage response with the instantaneous voltages from the two remaining sensors (figure 2), it was possible to determine all the turbulence-stress-tensor components $\overline{w_i w_j}$ and turbulent heat fluxes $\overline{w_i \vartheta}$. The rearrangement of these quantities into a spatially fixed coordinate system y_p was made via transformation rules

$$\left.\begin{aligned} \overline{u_p u_q} &= \overline{w_i w_j} e_{pi} e_{qj}, \\ \overline{u_p \vartheta} &= \overline{w_i \vartheta} e_{pi}, \end{aligned}\right\} \quad (u_1 \equiv u_x; \quad u_2 \equiv u_r; \quad u_3 = u_\varphi),$$

where the transformation matrix takes the form

$$e_{pi} = \begin{vmatrix} \cos\alpha\cos\varphi & -\sin\varphi & -\sin\alpha\cos\varphi \\ \cos\alpha\sin\varphi & \cos\varphi & -\sin\alpha\sin\varphi \\ \sin\alpha & 0 & \cos\alpha \end{vmatrix}.$$

Mean and fluctuating temperatures $\overline{\Theta}$ and ϑ, were measured simultaneously with the turbulent correlation measurement by using a 1 μm diameter 55P31 resistance thermometer operated by the 55 M 20 temperature bridge (figure 2). The estimation of measurement accuracy has been given in detail by Kurzak (1982), where the maximum errors in this experiment were estimated to be about $\mp 0.6\,\%$ for the mean velocity, less than $\mp 0.5\,\%$ for the mean temperature; about $\mp 8\,\%$ for the r.m.s. values of turbulent fluctuations, and about $\mp 12\,\%$ for the turbulent fluxes. However, it should be emphasized that all the values given above are the maximum ones and do not necessarily occur during the experiment. This may be proved by the fact that the empirical results have not shown greater scatter but are gathered about the common curves.

3. Flow characteristics at the exit plane

The full documentation of the flow field at the exit plane is given in figures 3 and 4 for the non-swirling jet and for the maximum swirling jet, respectively. In order to accentuate flow phenomena in the boundary layer, the abscissae in figures 3(*a*) and 4(*a*) have been scaled up in the region close to the nozzle wall.

The distributions of mean and turbulent quantities for the non-swirling jet (figure 3(*a*)) are quite typical and there is no need to discuss them in detail. However, it is worth noting that the thermal-boundary-layer thickness δ_Θ is greater than δ estimated from the velocity distribution. This may be attributed to the cooling effect of the nozzle wall. At the same time, the $\overline{U}_x$ profile plotted in figure 3(*b*) in the usually applied dimensionless form $\overline{U}_x^+ = f(y^+)$ demonstrates the laminar character of the exit boundary layer.

The flow characteristics corresponding to the maximum swirl degree (figure 4*a*) are much more interesting. Close to the jet axis an obvious mean-axial-velocity deficit appears, caused by the swirl action. However, at $s = 0.42$ the reverse flow has not yet been observed. In contrast to Komori & Ueda's (1985) findings the mean-temperature profile does not exhibit a similar decrement at the jet axis. This may be ascribed partially to the lower swirl number in the present experiment, and partially to the different method of swirl generation. The longitudinal Reynolds stress $\overline{u_x^2}$ has two distinct peaks located approximately in the regions of maximum axial velocity gradient. The distribution of tangential Reynolds stress $\overline{u_\varphi^2}$ exhibits a similar character. The profile of temperature variance $\overline{\vartheta^2}$ shows, however, only one peak,

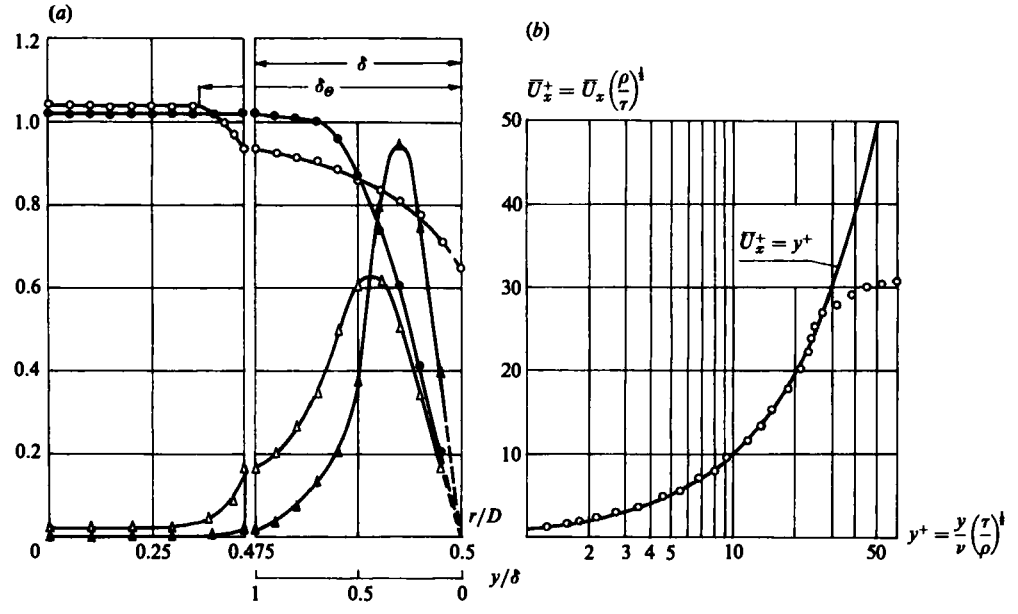

FIGURE 3. (*a*) Flow characteristics at the exit plane of the unswirled jet at $\overline{\Theta}_{ave} = 40°$: ●, $\overline{U}_x/\overline{U}_{ave}$; ○, $\overline{\Theta}/\overline{\Theta}_{ave}$; ▲, $\overline{u}_x^2/\overline{U}_{ave}^2 \times 10$; △, $\overline{\vartheta}^2/\overline{\Theta}_{ave}^2 \times 10^2$. (*b*) Mean-velocity profile in the exit boundary layer: $\Theta_{ave} = 40°$, $x/D = 0, s = 0$.

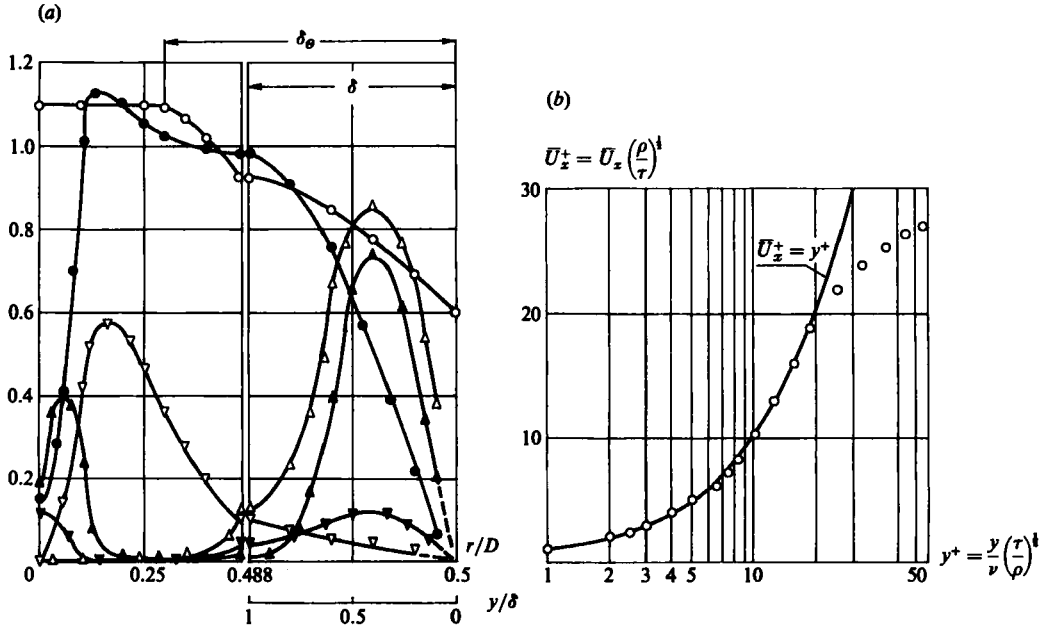

FIGURE 4. (*a*) Flow characteristics at the exit plane of the swirling jet ($s = 0.42$) at $\overline{\Theta}_{ave} = 40°$: ●, $\overline{U}_x/\overline{U}_{ave}$; ▽, $\overline{U}_\varphi/\overline{U}_{ave}$; ○, $\overline{\Theta}/\overline{\Theta}_{ave}$; ▲, $\overline{u}_x^2/\overline{U}_{ave}^2 \times 10$; ▼, $\overline{u}_\varphi^2/\overline{U}_{ave}^2 \times 10^2$; △, $\overline{\vartheta}^2/\overline{\Theta}_{ave}^2 \times 10^2$. (*b*) Mean-velocity profile in the exit boundary layer: $\Theta_{ave} = 40°$, $x/D = 0$, $s = 0.42$.

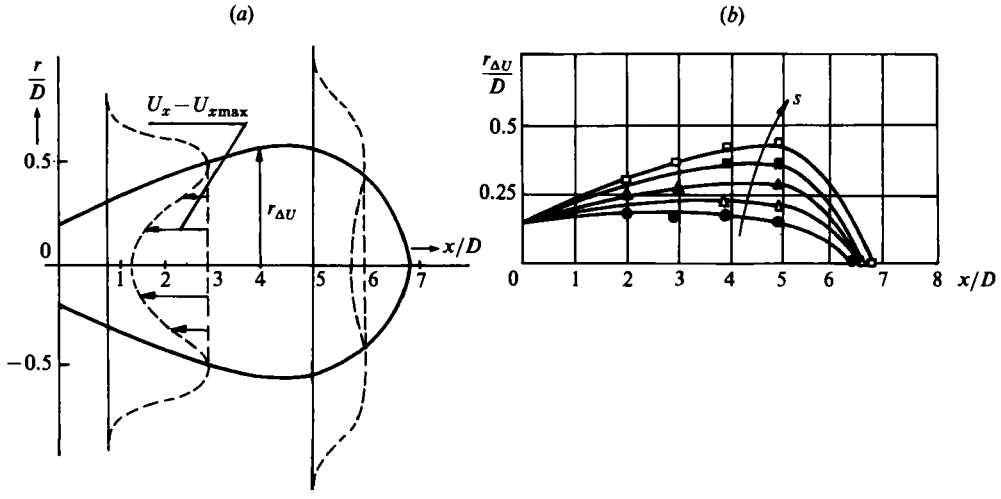

FIGURE 5. (*a*) Shape of the deformation bubble in the swirling jet; (*b*) influence of swirl on its spatial extent: ●, $s = 0.22$; △, 0.31; ▲, 0.33; ■, 0.36; □, 0.42.

located near the nozzle wall, where the mean-temperature gradient has a non-zero value. The axial velocity distribution $\overline{U}_x^+ = f(y^+)$, shown in figure 4(*b*), also seems to testify to the laminar character of flow in the nozzle boundary layer.

4. Evolution of mean-velocity and mean-temperature fields

At the exit plane of a swirling jet (figure 4*a*) we have observed the characteristic deformation of the axial mean-velocity distribution, which reveals itself in the creation of an M-type velocity profile. It is interesting to note that in a near-flow region, the volume containing M-type velocity profiles takes the shape of a characteristic 'deformation bubble', as shown in figure 5(*a*). With an increase of swirl, its longitudinal extent grows only slightly, while at the same time the radial dimension of the bubble is enlarged much more distinctly (figure 5*b*). It is conceivable that the strong radial velocity gradient occurring in that zone could lead to a considerable intensification of all the turbulent transport processes. This tendency will be proved later.

Figure 6 shows the variation of axial-mean-velocity half-width b and mean-temperature half-width b_θ defined by the relations

$$\overline{U}_x(b) = 0.5\overline{U}_{x\max}; \quad \overline{\Theta}(b_\theta) = 0.5\overline{\Theta}_{\max}.$$

For the mean flow region of the swirling jets with the $\overline{U}_x$ maximum displaced from the jet axis, b was taken as an outer value of the radius at which the mean velocity equals one half of its maximum value. Further downstream both those scales appear to be linear functions of the x-coordinate:

$$b = \frac{B}{D}[x - x_0(s)],$$

$$b_\theta = \frac{B_\theta}{D}[x - x_0(s)],$$

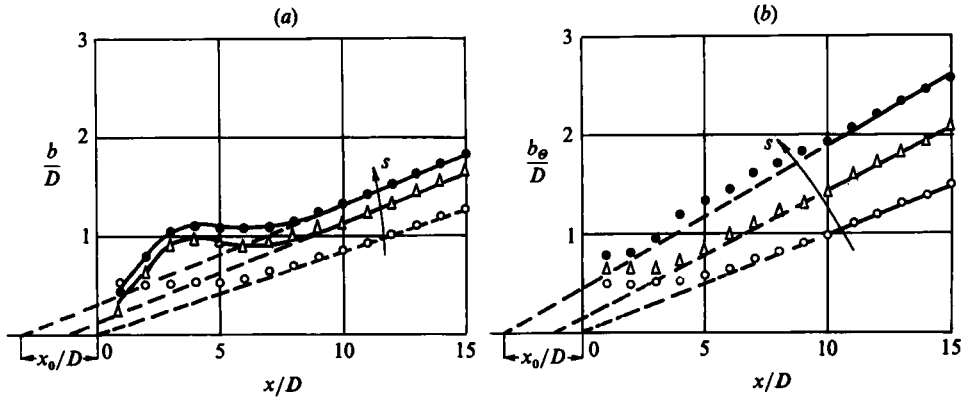

FIGURE 6. Radial spread of the jet at $\overline{\theta}_{ave} = 40°$ (○, $s = 0$; △, 0.31; ●, 0.42): (*a*) mean-velocity half-width; (*b*) mean-temperature half-width.

Source	Swirl degree	x_0/D
Wygnanski & Fiedler (1969)	0	+3, for $x/D < 50$ +7, for $x/D > 50$
Chigier & Chervinsky (1967)	0.23	−3, independent of s
Pratte & Keffer (1972)	0; 0.3	−3, independent of s
Traugott (1958)	0.13; 0.35	−3, independent of s
Curtet & Darigol (1978)	0–1.58	$-5.4s$ for $\overline{U}_x$ distribution $-2.8s$ for $\overline{\theta}$ distribution
Grandmaison & Becker (1982)	0; 0.22–0.68	+3.4 for $s = 0$ −6.8 for $s = 0.22$ and $s = 0.36$

TABLE 1. The effect of the swirl degree on the virtual origin of the flow

where x_0 determines the localization of the so-called virtual origin of flow, being dependent on the swirl degree according to relation

$$\frac{x_0}{D} = B_s s; \quad B_s = -3.5.$$

There are divergent opinions as to what extent the position of the virtual origin of the flow is affected by swirl degree (see table 1). Our results, as expressed by the above relation, are in qualitative agreement with the data given by Curtet & Darigol, and do not confirm the independence of x_0 of swirl degree, as suggested by other authors, mentioned in table 1. The parameters B and B_θ are also slightly increasing functions of swirl, as shown in figure 7 where the results of this experiment are compared with the data of Chigier & Chervinsky (1967) and Grandmaison & Becker (1982). Summing up this part of the experimental data, it may be stated that, according to numerous opinions supported by the results given in figure 6(*a*), the swirl increases the lateral spread of the jet owing to the larger entrainment of fluid from the ambient surroundings towards the jet. This is especially evident in the near flow region, say for $x/D < 5$.

At the same time, a comparison of the characteristic lengthscales b and b_θ shows that in the whole flow region $b_\theta > b$. Such a phenomenon, which has already been

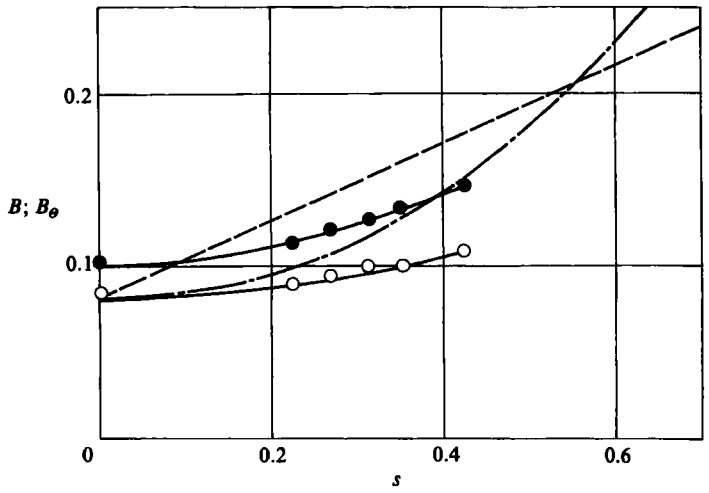

FIGURE 7. Variation of parameters B and B_θ with swirl at $\overline{\theta}_{ave} = 40°$: ○, B; ●, B_θ – present results; —·—·—, $B(s)$ after Grandmaison & Becker (1982); — — —, $B(s)$ after Chigier & Chervinsky (1967).

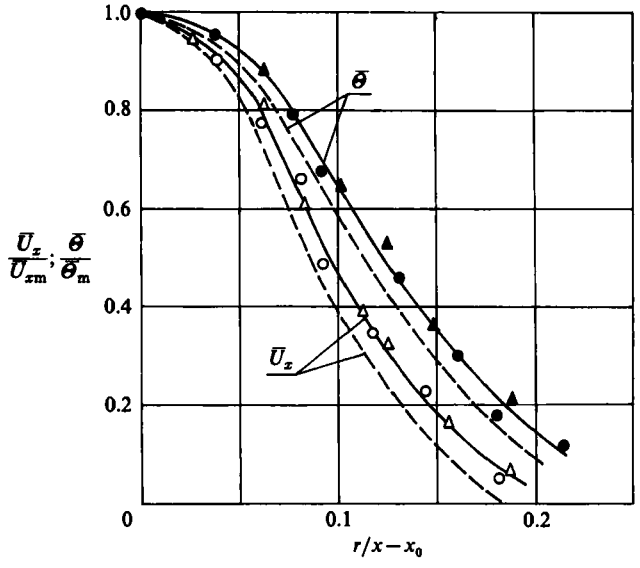

FIGURE 8. Comparison of $\overline{U}_x/\overline{U}_{xm}$ and $\overline{\theta}/\overline{\theta}_m$ profiles across the swirling jet at $s = 0.31$ and $\overline{\theta}_{ave} = 40°$ for $x/D = 9$ – ○, $\overline{U}_x/\overline{U}_{xm}$; ●, $\overline{\theta}/\overline{\theta}_m$; and for $x/D = 15$ – △, $\overline{U}_x/\overline{U}_{xm}$; ▲, $\overline{\theta}/\overline{\theta}_m$; — — —, after Komori & Ueda (1984) for $s = 0$, $x/d > 50$.

observed at the nozzle exit (figures 3*a* and 4*a*), is also confirmed in figure 8 where $\overline{U}_x/\overline{U}_{xm}$ and $\overline{\theta}/\overline{\theta}_m$ profiles have been plotted against the relative coordinate $r/(x-x_0)$ and compared with the results of Komori & Ueda (1984) for an unswirled jet injected into a low-speed coflowing stream.

It is reasonable to expect that, according to the self-preservation hypothesis, the mean-velocity and mean-temperature profiles expressed in non-dimensional forms $\overline{U}_x/\overline{U}_{x\,max}$ and $\overline{\theta}/\overline{\theta}_{max}$ in terms of a relative coordinate $\eta = r/b$ (where b is a suitably chosen lengthscale) should exhibit some similarity in a far flow region. This tendency

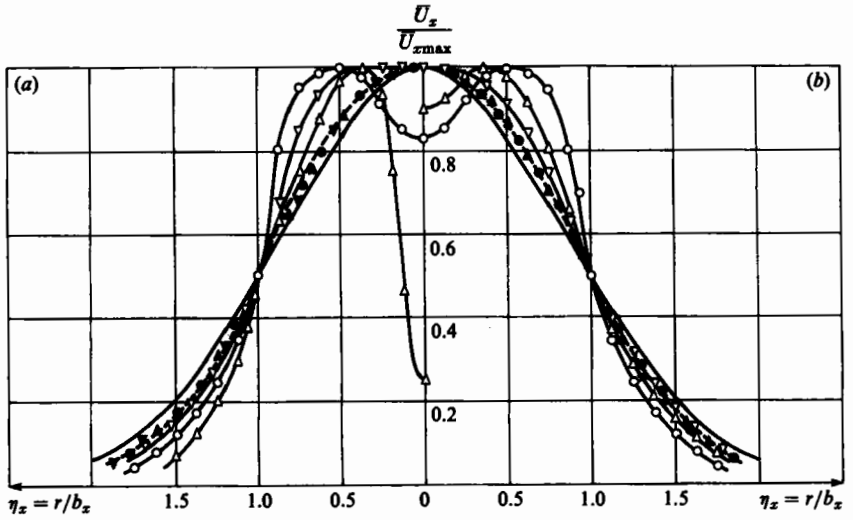

FIGURE 9. Normalized radial distributions of $\overline{U}_x$ at $\overline{\Theta}_{ave} = 40°$ for (*a*) various swirl degrees: $x/D = 1$ – ▽, $s = 0$; ○, 0.31; △, 0.42 and $x/d = 9$ – ▼, $s = 0$; ●, 0.31; ▲, 0.42; and (*b*) various axial distances at $s = 0.31$: ○, $x/D = 1$; △, 5; ▽, 7; ●, 9; ▲, 15. Gaussian error curve: $\overline{U}_x/\overline{U}_{x\max} = \exp(\eta_x^2 \ln 2)$.

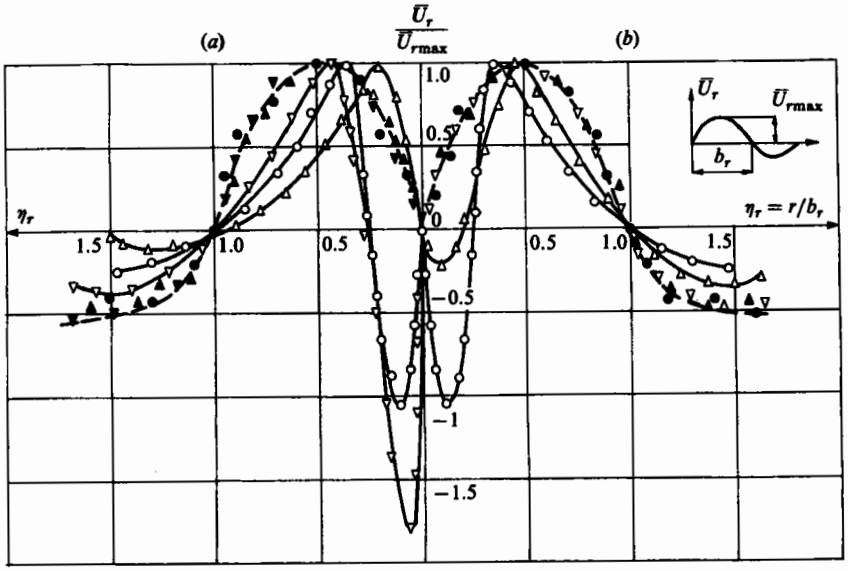

FIGURE 10. Normalized radial distributions of $\overline{U}_r$ at $\overline{\Theta}_{ave} = 40°$ for (*a*) various swirl degrees: $x/D = 3$ – △, $s = 0$; ○, 0.31; ▽, 0.42; and $x/D = 7$ – ▲, $s = 0$; ●, 0.31; ▼, 0.42; and (*b*) various axial distances at $s = 0.31$; ○, $x/D = 3$; △, 5; ●, 7; ▽, 9; ▲, 15.

is proved in figures 9–12, which illustrate both the influence of swirl degree at the given cross-section (left-hand sides of the figures) and the downstream evolutions of the mean-flow quantities at the medium swirl degree $s = 0.31$ (right-hand sides of the figures).

Figure 9 shows that the greater the swirl degree the more distinct is the $\overline{U}_x$ deficit at the jet axis observed inside the deformation bubble (figure 5). Starting with the

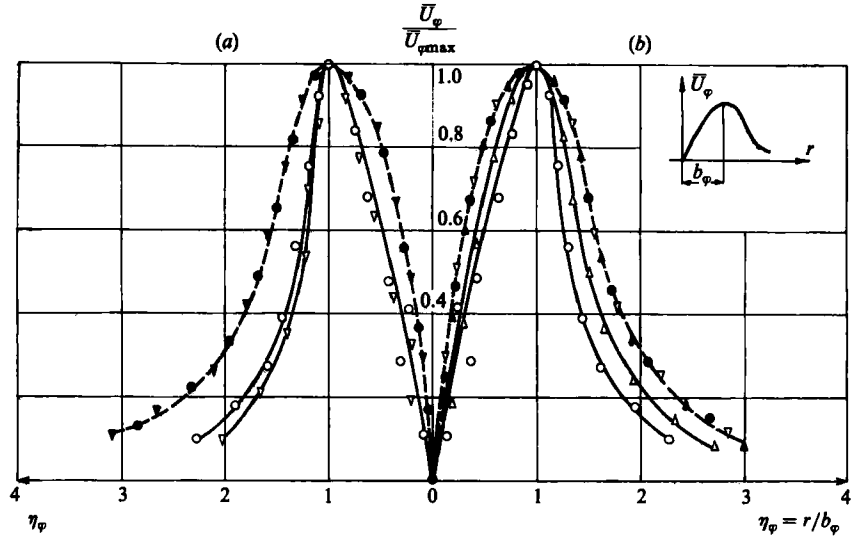

FIGURE 11. Normalized radial distributions of $\overline{U}_\varphi$ at $\overline{\Theta}_{ave} = 40°$ for (*a*) various swirl degrees: $x/D = 1$ – ○, $s = 0.31$; ▽, 0.42; and $x/D = 7$ – ●, $s = 0.31$; ▼, 0.42; and (*b*) various axial distances at $s = 0.31$: ○, $x/D = 1$; △, 5; ●, 7; ▽, 9; ▲, 15.

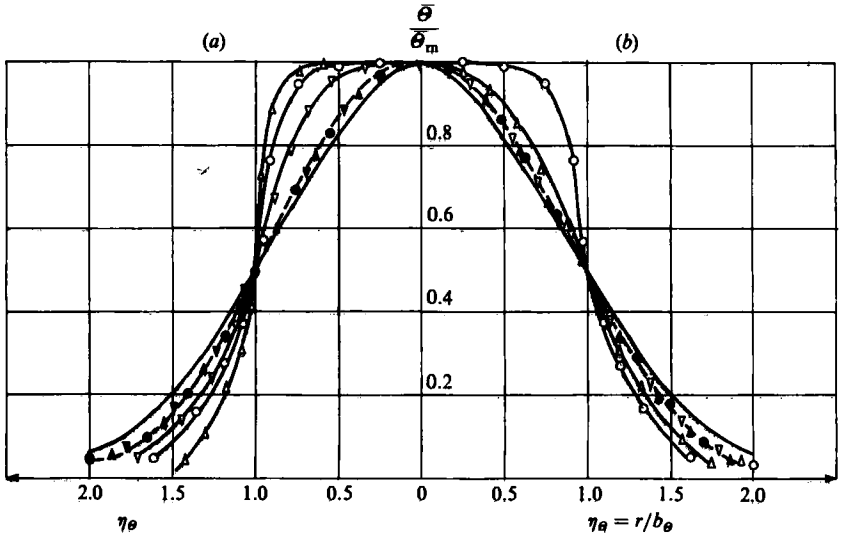

FIGURE 12. Normalized radial distributions of $\overline{\Theta}$ at $\overline{\Theta}_{ave} = 40°$ for (*a*) various swirl degrees: $x/D = 1$ – △, $s = 0$; ○, 0.31; ▽, 0.42; and $x/D = 7$ – ▲, $s = 0$; ●, 0.31; ▼, 0.42; and (*b*) various axial distances at $s = 0.31$; ○, $x/D = 1$; △, 5; ●, 7; ▽, 9; ▲, 15: ——, Gaussian error curve $\overline{\Theta}/\overline{\Theta}_m = \exp(\eta_\Theta^2 \ln 2)$.

distance $x/D \approx 9$, the mean-axial-velocity distributions, irrespective of swirl degree, tend to attain a common universal profile close to the Gaussian error curve.

The distributions of the mean-radial-velocity component are presented in figure 10 in terms of the coordinate $\eta_r = r/b_r$, where b_r denotes the outer radius at which $\overline{U}_r = 0$. In the non-swirling jet $\overline{U}_r$ has a positive value in the central core, representing an outflow, and a negative value in the outer jet region, consistent with the direction of the entrained fluid. In the near flow field of the swirling jets, $\overline{U}_r$ twice changes its

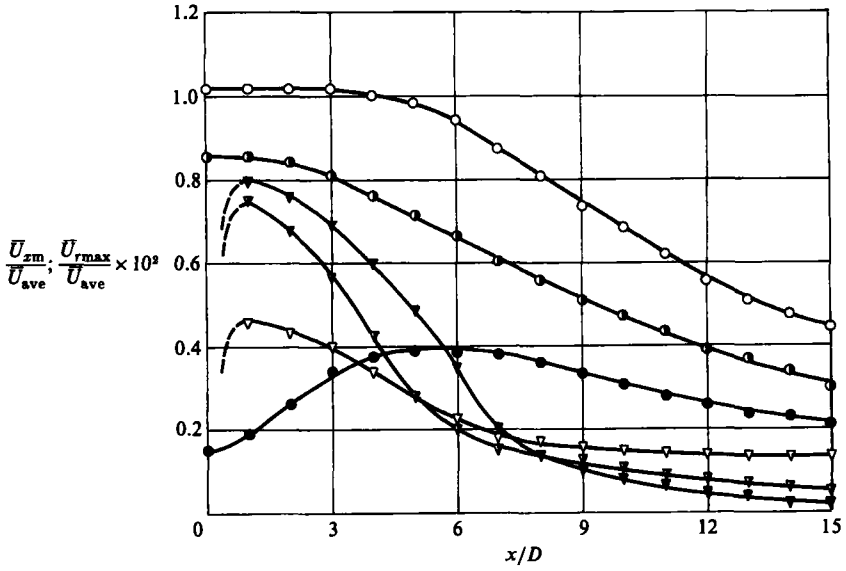

FIGURE 13. Downstream evolution of $\overline{U}_{xm}/\overline{U}_{ave}$ and $\overline{U}_{r\,max}/\overline{U}_{ave}$ at $\overline{\Theta}_{ave} = 40°$ for various swirl degrees: $\overline{U}_x$ – ○, $s = 0$; ◑, 0.31; ●, 0.42; and $\overline{U}_r$ – ▽, $s = 0$; ▼, 0.31; ▼, 0.42.

sign and for $\eta_r \lesssim 0.25$ shows negative values due to the mass flux towards the jet axis which is to equalize the axial velocity deficit inside the deformation bubble. In the far flow region, $\overline{U}_r$ distributions, independently of swirl degree, seem to group fairly well about the common curve (broken line in figure 10). The same tendency towards the self-similar profile may be observed in the tangential velocity distributions shown in figure 11.

Mean-temperature profiles presented in figure 12 exhibit a hat-like shape close to the nozzle and a tendency to a universal Gaussian curve further downstream. However, in contrast to the results obtained by Komori & Ueda (1985), no temperature minimum at the jet axis was observed in the near flow region.

The downstream evolution of the axial-mean-velocity component measured at the jet axis (figure 13), shows that in the non-swirling case $\overline{U}_{xm}$ remains constant within the potential core up to $x/D \approx 3$. For maximum swirl degree $\overline{U}_{xm}$ grows inside the deformation bubble and decays further downstream. The decay of the maximum radial-mean-velocity component is also shown in figure 13. The values of $\overline{U}_{r\,max}$ are at least two orders of magnitude smaller than the maximum streamwise component. With the growth of swirl degree they tend to increase in the range $x/D < 5$ and to decrease further downstream.

The decay of the maximum swirl velocity $\overline{U}_{\varphi max}$ is shown as a function of x/D in figure 14. It is worth noticing that for all the values of swirl degree the experimental results, normalized by $(\overline{U}_{x\,max})_0$ measured at the exit plane, lie on almost the same curve and in the distance $x/D > 7$ are in close agreement with results obtained by Chigier & Chervinsky (1967).

The downstream evolution of maximum mean temperature $\overline{\Theta}_{max} = \overline{\Theta}_m$ is presented in figure 15. In the non-swirling jet, $\overline{\Theta}_m$ remains constant within the potential core as for the $\overline{U}_{xm}$ distribution given in figure 12. The swirl action leads to the faster decay of $\overline{\Theta}_m$, which in the distance $x/D > 4$ is in qualitative agreement with the data given by Komori & Ueda (1985). For additional comparison, in figure 15 the results

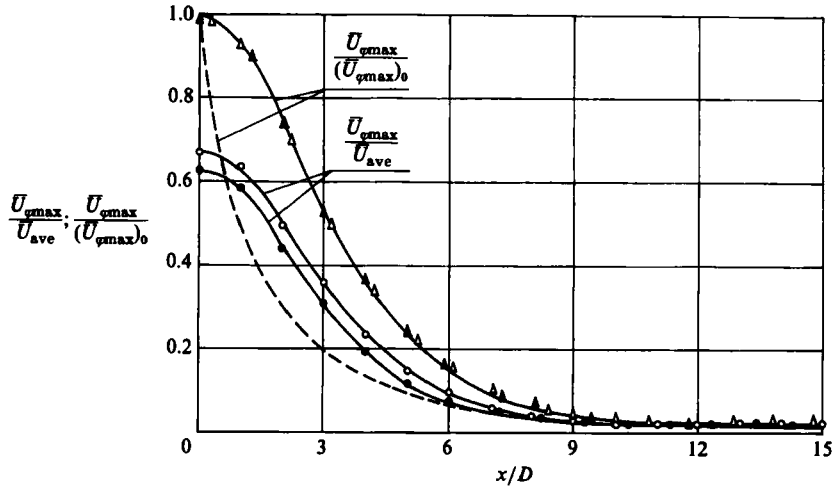

FIGURE 14. Normalized axial distributions of $\overline{U}_{\varphi max}$ at $\overline{\Theta}_{ave} = 40°$ for two swirl degrees: ○, △, $s = 0.31$; ●, ▲, $s = 0.42$; ———, after Chigier & Chervinsky (1967).

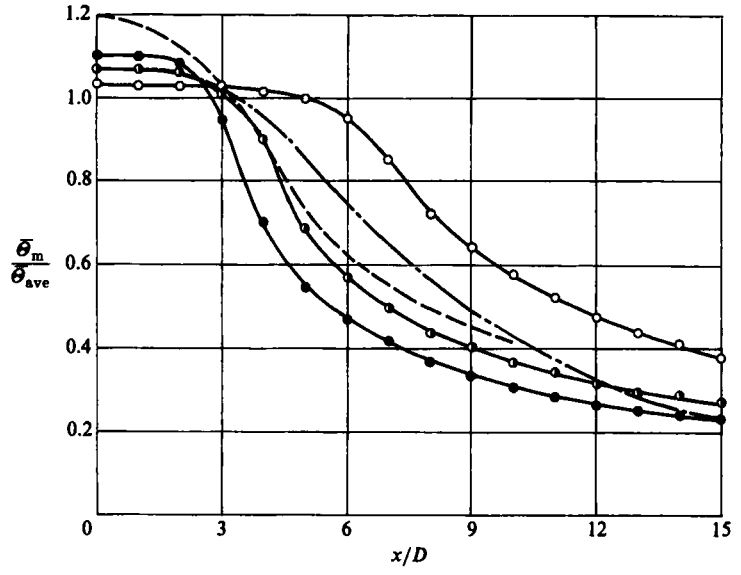

FIGURE 15. Downstream evolution of $\overline{\Theta}_m/\overline{\Theta}_{ave}$ at $\overline{\Theta}_{ave} = 40°$ for various swirl degrees: ○, $s = 0$; ◑, 0.31; ●, 0.42; ———, after Komori & Ueda (1984) for $s = 0.2$, $\overline{\Theta}_{ave} = 20°$; —·—·—, after Tkackaja & Ustimienko (1971) for $s = 0.26$, $\overline{\Theta}_{ave} \approx 28°$.

of Tkackaja & Ustimienko (1971) have also been plotted. They were rearranged on the assumption that $\overline{\Theta}_{ave} = 280°$ is equal to a value 0.93 times as large as the maximum temperature $(\overline{\Theta}_{max})_0$ at the nozzle exit plane. The swirl intensity $(\overline{U}_{\varphi max}/\overline{U}_{x max})_0 = 0.137$ used in Tkackaja & Ustimienko's experiment was found to correspond to a value $s \approx 0.26$. As one can see, in spite of the much higher jet temperature, its downstream evolution is in qualitative agreement with that found in the present investigations.

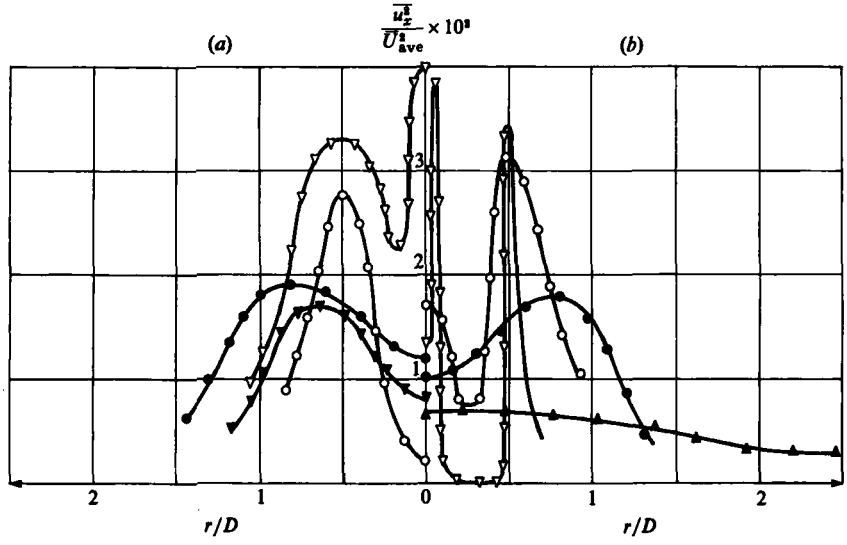

FIGURE 16. Normalized radial distributions of $\overline{u_x^2}$ at $\overline{\Theta}_{ave} = 40°$ for (*a*) various swirl degrees: $x/D = 3$ – ○, $s = 0$; ▽, 0.42 and $x/D = 7$ – ▼, $s = 0$; ●, 0.42; and (*b*) various axial distances at $s = 0.31$: ▽, $x/D = 1$; ○, 3; ●, 7; ▲, 15.

5. Distributions of turbulent quantities

5.1. *Turbulence-stress-tensor components*

The measurements of mean-flow quantities presented above indicate that their radial distributions become reasonably self-preserving some few diameters downstream of the nozzle. However, the turbulent quantities show marked departures from self-preservation in that region, because, as concluded by Townsend (1956), the effect of initial conditions diminishes rather slowly with distance downstream. As our measurements were not made far enough downstream to attain self-preservation of turbulent motion, reported radial distributions of turbulent quantities presented in figures 16–20 were plotted in terms of the relative radial coordinate r/D.

The swirl action causes an increase of all the turbulence-stress-tensor components in the near flow region (see left-hand sides of figures 16–20) and a decrease outside the region influenced by the deformation bubble. At the stations $x/D = 1$ and 3 the radial distributions of $\overline{u_x^2}$ (figure 16) exhibit the presence of two peaks, observed earlier at the exit plane (figure 4*a*). Further downstream they merge and form one maximum that moves towards the jet axis with the increase of coordinate x.

The distributions of $\overline{u_r^2}$ and $\overline{u_\varphi^2}$ shown in figures 17 and 18 exhibit a similar tendency. However, both the lateral components are everywhere less than the streamwise one, which agrees with the measurements of Wygnanski & Fiedler (1969) for non-swirling jets, and with the data of Pratte & Keffer (1972) for swirling jets.

Figures 19 and 20 show profiles of turbulent shear stresses $\overline{u_x u_r}$ and $\overline{u_r u_\varphi}$, respectively. At the first two stations of the swirling jets ($x/D = 1$ and 3) $\overline{u_x u_r}$ is negative near the jet axis. This corresponds to the positive velocity gradient $\partial \overline{U}_x/\partial r$ inside the deformation bubble (figure 5) and indicates that the momentum is transported towards the central axis. However, this peculiarity is not observed in $\overline{u_r u_\varphi}$ distributions. In the outer part of the near swirling jet, $\overline{u_x u_r}$ attains positive values, large when compared with those in the non-swirling flow. This means that

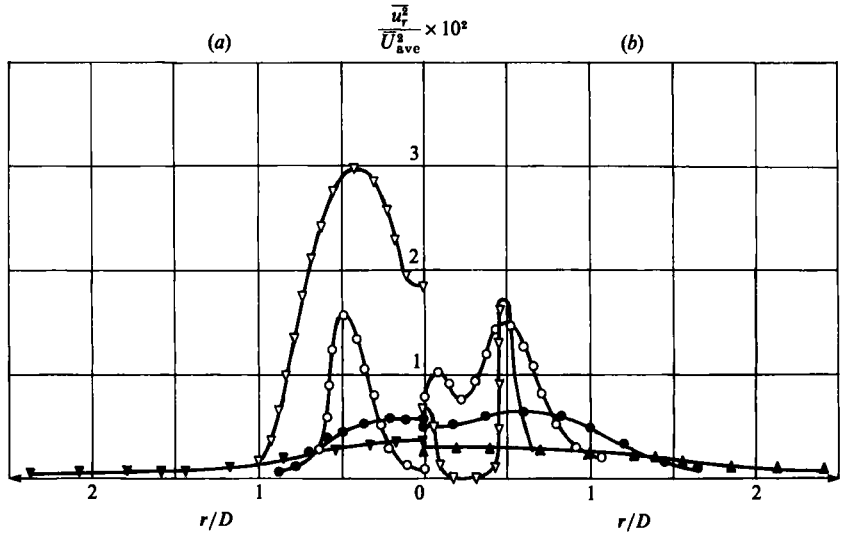

FIGURE 17. Normalized radial distributions of $\overline{u_r^2}$ at $\overline{\theta}_{ave} = 40°$ for (*a*) various swirl degrees: $x/D = 3$ – ○, $s = 0$; ▽, 0.42; $x/D = 7$ – ●, $s = 0$; ▼, 0.42; and (*b*) various axial distances at $s = 0.31$: ▽, $x/D = 1$; ○, 3; ●, 7; ▲, 9.

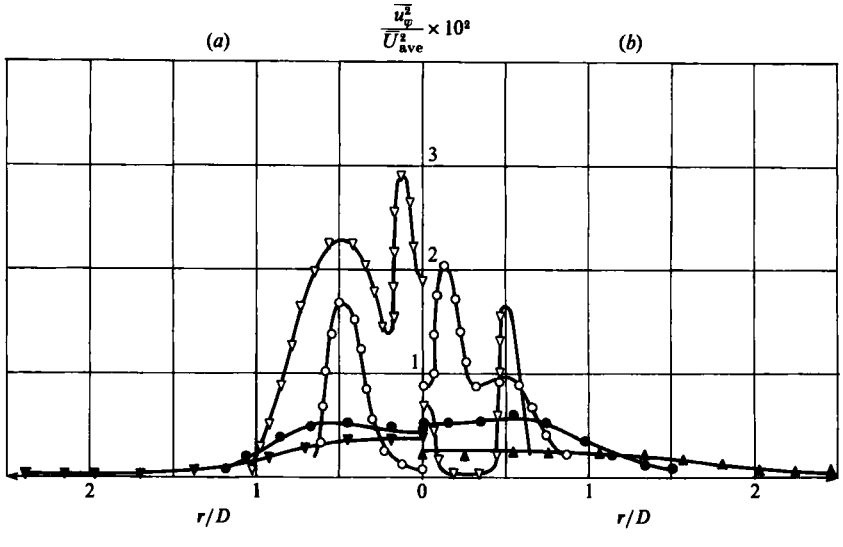

FIGURE 18. Normalized radial distributions of $\overline{u_\varphi^2}$ at $\overline{\theta}_{ave} = 40°$ for (*a*) various swirl degrees: $x/D = 3$ – ○, $s = 0$; ▽, 0.42; and $x/D = 7$ – ●, $s = 0$; ▼, 0.42; and (*b*) various axial distances at $s = 0.31$: ▽, $x/D = 1$; ○, 3; ●, 7; ▲, 9.

the swirl action here intensifies the momentum transfer towards the ambient fluid. For a given swirl degree the maximum values of $\overline{u_x u_r}$ decrease in the downstream direction and move towards the outer part of the jet as a result of its lateral spread. The momentum flux $\overline{u_r u_\varphi}$ is evidently smaller than $\overline{u_x u_r}$ and shows positive values within the whole range r/D. In the near flow region $\overline{u_r u_\varphi}$ is also strongly enhanced by swirl action. It is worth noting that in the far flow the radial distributions of $\overline{u_x u_r}$

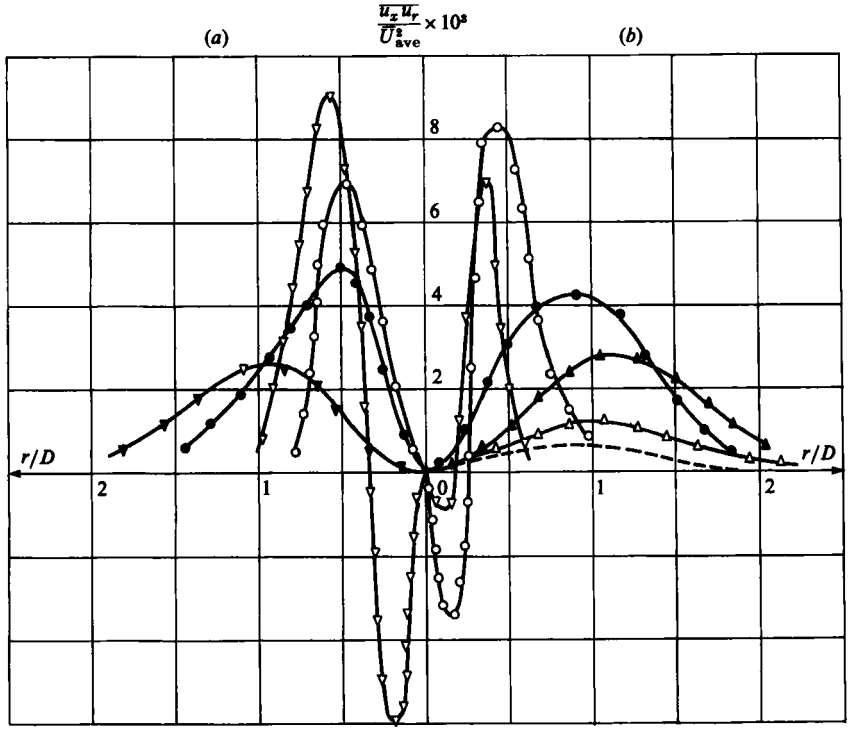

FIGURE 19. Normalized radial distributions of $\overline{u_x u_r}$ at $\overline{\theta}_{ave} = 40°$ for (*a*) various swirl degrees: $x/D = 3 - \bigcirc$, $s = 0$; $\bigtriangledown$, 0.42; and $x/D = 7 - \bullet$, $s = 0$; $\blacktriangledown$, 0.42; and (*b*) various axial distances at $s = 0.31$; $\bigtriangledown$, $x/D = 1$; $\bigcirc$, 3; $\bullet$, 7; $\blacktriangle$, 9; $\triangle$, 12; ———, after Pratte & Keffer (1972) for $x/D = 12$, $s = 0.3$.

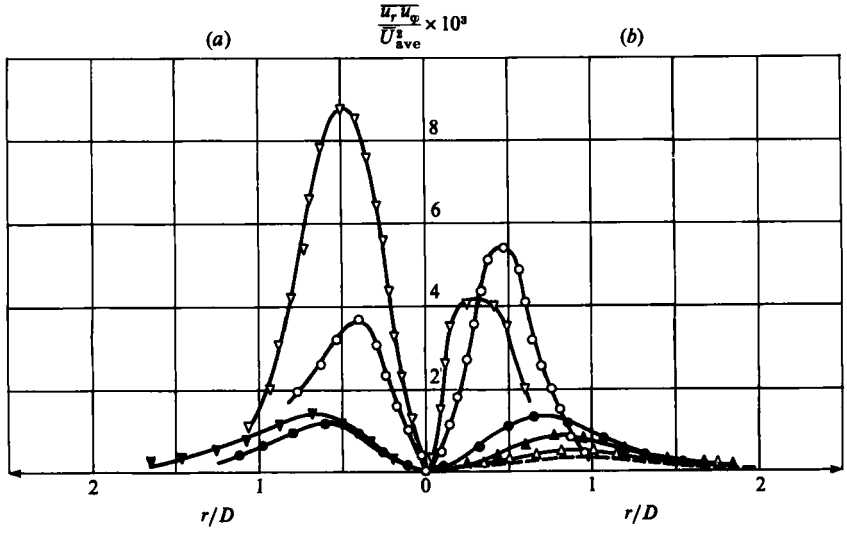

FIGURE 20. Normalized radial distributions of $\overline{u_r u_\varphi}$ at $\overline{\theta}_{ave} = 40°$ for (*a*) various swirl degrees: $x/D = 3 - \bigcirc$, $s = 0.22$; $\bigtriangledown$, 0.42; and $x/D = 7 - \bullet$, $s = 0$; $\blacktriangledown$, 0.42; and (*b*) various axial distances at $s = 0.31$: $\bigtriangledown$, $x/D = 1$; $\bigcirc$, 3; $\bullet$, 7; $\blacktriangle$, 9; $\triangle$, 12: ———, after Pratte & Keffer (1972) for $x/D = 12$, $s = 0.3$.

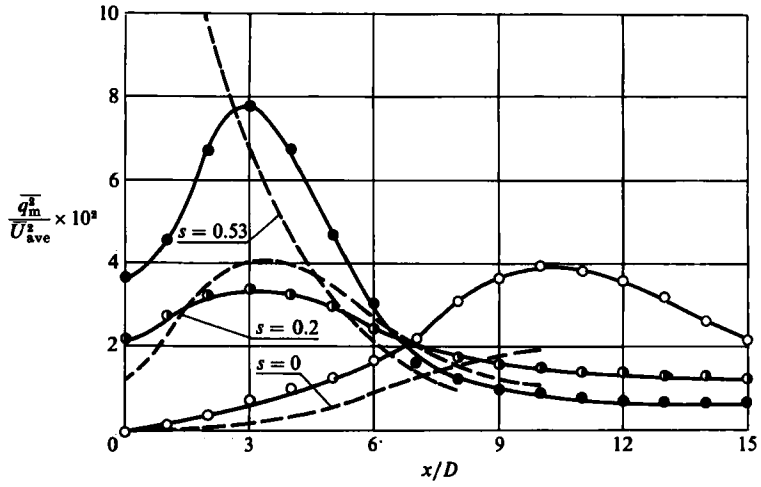

FIGURE 21. Downstream evolution of turbulent kinetic energy measured at the jet axis at $\overline{\Theta}_{ave} = 40°$: ○, $s = 0$; ◑, 0.31; ●, 0.42; ———, after Komori & Ueda (1985) for $s = 0$; 0.2 and 0.53 respectively.

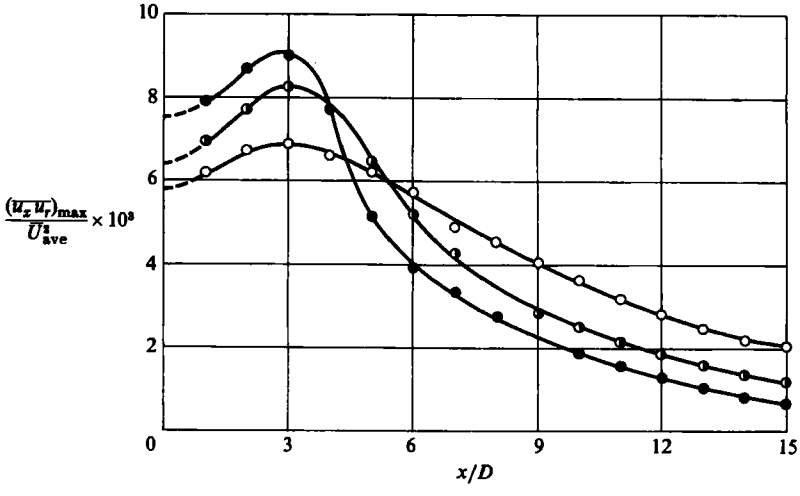

FIGURE 22. Downstream evolution of maximum Reynolds shear stress $\overline{u_x u_r}$ at $\overline{\Theta}_{ave} = 40°$: ○, $s = 0$; ◑, 0.31; ●, 0.42.

and $\overline{u_r u_\varphi}$ obtained in the present experiment correspond moderately well with the data of Pratte & Keffer (1972), plotted for comparison in figures 19 and 20.

Figure 21 illustrates to what extent the turbulence energy $\frac{1}{2}\overline{q^2} = 0.5(\overline{u_x^2} + \overline{u_r^2} + \overline{u_\varphi^2})$ measured at the jet axis is affected by the swirl degree. As can be seen, this effect is entirely different in the near and far flow regions of the jet. The rise of swirl causes a considerable increase of turbulence energy near the nozzle outlet and its faster drop over the distance $x/D > 7$. That observation is in full accordance with the results of Elsner & Musialik (1982) where the influence of swirl on particular terms of the turbulence energy equation was discussed. For comparison, figure 21 also shows the results predicted by Komori & Ueda (1985) in their numerical calculations of the slightly heated jet issuing into a low-speed coaxial flow.

A similar tendency towards an increase of turbulent shear stresses $(\overline{u_x u_r})_{max}$ and

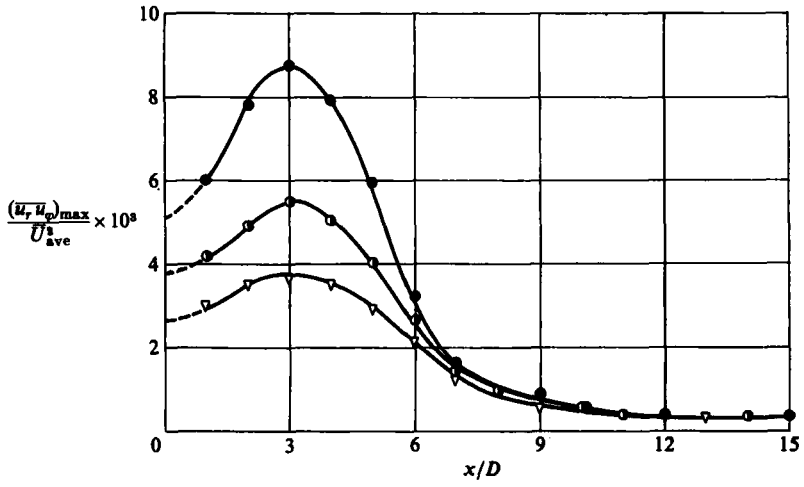

FIGURE 23. Downstream evolution of maximum Reynolds shear stress $\overline{u_r u_\varphi}$ at $\overline{\Theta}_{ave} = 40°$: ▽, $s = 0.22$; ◑, 0.31; ●, 0.42.

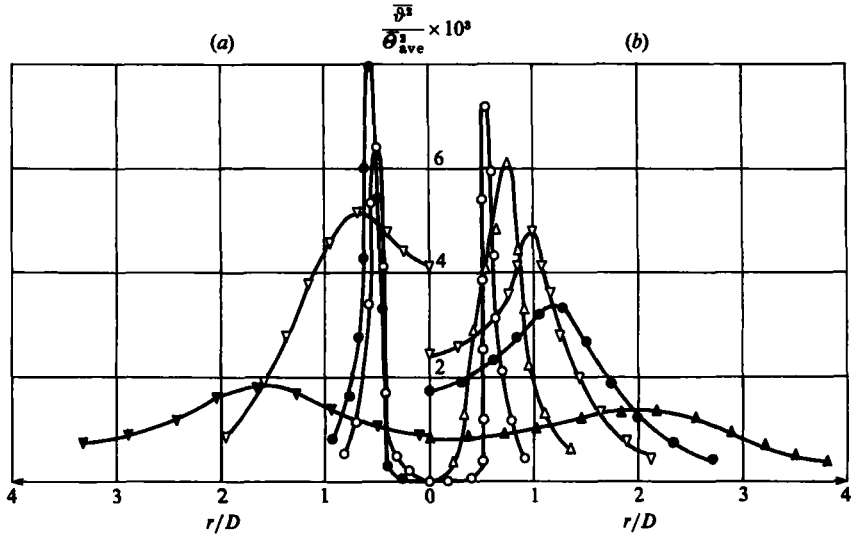

FIGURE 24. Normalized radial distributions of the mean-square value of temperature fluctuations at $\overline{\Theta}_{ave} = 40°$ for (*a*) various swirl degrees: $x/D = 1$ – ○, $s = 0$; ●, 0.42; $x/D = 7$ – ▽, $s = 0$; ▼, 0.42; and (*b*) various axial distances at $s = 0.31$: ○, $x/D = 1$; △, 3; ▽, 5; ●, 7; ▲, 15.

especially $(\overline{u_r u_\varphi})_{max}$ in a near flow region under the swirl action is also illustrated in figures 22 and 23. The growth of swirl leads next to the faster decay of both these stresses further downstream, so that $(\overline{u_x u_r})_{max}$ related to the swirling jets finally reaches a lower level than that corresponding to an unswirled jet. It is worth mentioning that analogous behaviour of $\overline{u_x u_r}$ stress in the swirling jet was also observed by Allen (1970).

5.2. *Temperature fluctuations and turbulent heat flux*

Radial distributions of the mean-square value of temperature fluctuations are illustrated in figure 24. In the area close to the nozzle exit (station $x/D = 1$) the swirl

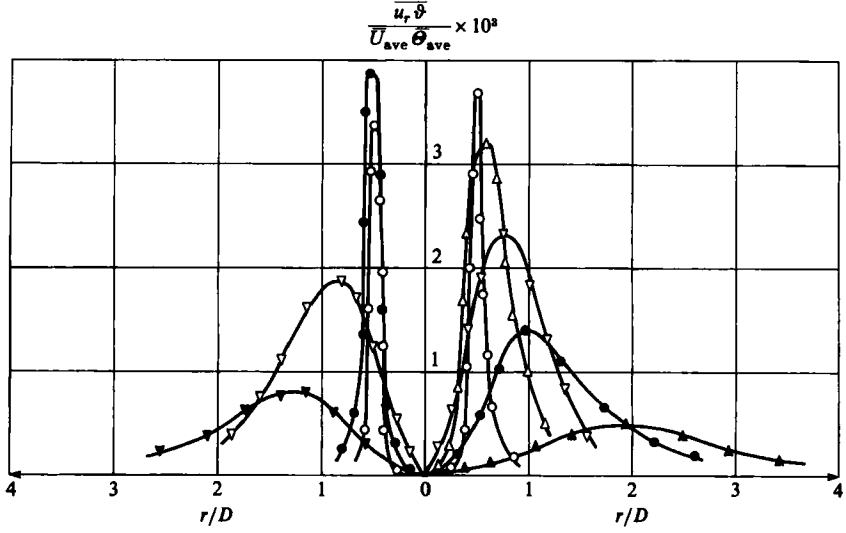

FIGURE 25. Normalized radial distributions of turbulent heat flux $\overline{u_r\vartheta}$ at $\overline{\Theta}_{ave} = 40°$ for (a) various swirl degrees: $x/D = 1$ – ○, $s = 0$; ●, 0.42; and $x/D = 7$ – ▽, $s = 0$; ▼, 0.42; and (b) various axial distances at $s = 31$: ○, $x/D = 1$; △, 3; ▽, 5; ●, 7; ▲, 15.

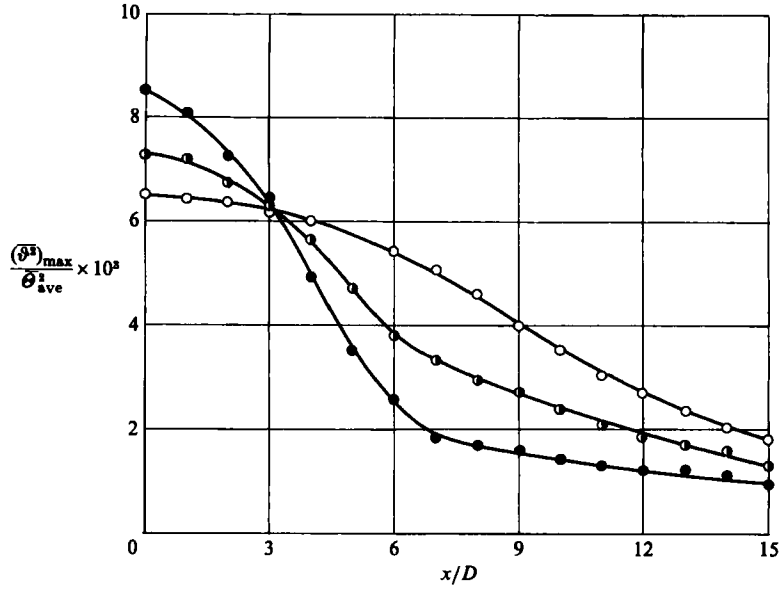

FIGURE 26. Downstram evolution of $(\overline{\vartheta^2})_{max}$ at $\overline{\Theta}_{ave} = 40°$ for various swirl degrees: ○, $s = 0$; ◑, 0.31; ●, 0.42.

causes the rise of $\overline{\vartheta^2}$ in the whole cross-section of the jet, (figure 24a), whereas further downstream ($x/D = 7$) it brings about the decrease of the maximum value of temperature variance and its slight growth in the external zone of the jet, resulting from its faster spread promoted by swirl action. For a given swirl degree (figure 24b) the maxima of $\overline{\vartheta^2}$ profiles decay with the axial distance and shift away from the jet axis.

When considering turbulent heat fluxes, special attention should be paid to the

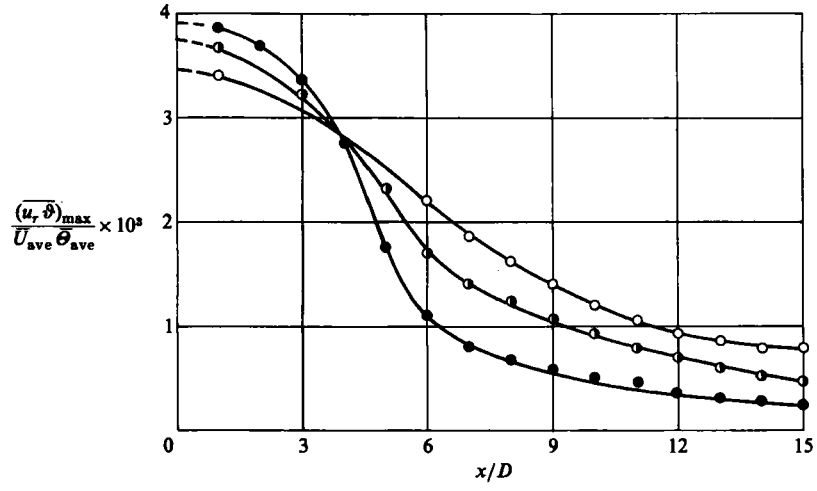

FIGURE 27. Downstream evolution of $(\overline{u_r\vartheta})_{max}$ at $\overline{\Theta}_{ave} = 40°$ for various swirl degrees: ○, $s = 0$; ◑, 0.31; ●, 0.42.

radial direction in which the gradients of $\overline{U}$ and $\overline{\Theta}$ reach their maximum values; hence, only the correlation $\overline{u_r\vartheta}$ is further discussed. Sample distributions presented in figure 25 show that $\overline{u_r\vartheta}$ is positive in the whole flow region. This means that, owing to the turbulent diffusion, the heat is transported always towards the ambient fluid. It should be mentioned that Komori & Ueda (1985) found a small area of negative $\overline{u_r\vartheta}$-values near the exit plane of a swirling jet caused by the positive mean-temperature gradient $\partial\overline{\Theta}/\partial r$ close to the central axis. Such a phenomenon has not, however, been observed in the present experiment.

The downstream evolutions of $(\overline{\vartheta^2})_{max}$ and $(\overline{u_r\vartheta})_{max}$ presented in figures 26 and 27 confirm once more the quite different effect of swirl in the near and far flow regions. It is interesting to note that the curves plotted in both these figures intersect at approximately the same point determined by the coordinate $x/D = 3$–4.

5.3. *Coefficients of turbulent momentum and heat diffusion*

Turbulent momentum diffusion in the swirling jets exhibits a fully anisotropic character and therefore the eddy-viscosity coefficient ν_T cannot be determined by a scalar relationship. Although, for example, Kubo & Guldin (1985) have assumed in their numerical calculations that ν_T may be treated as a scalar value, two different expressions are more often used:

$$\nu_{Trx} = \frac{\overline{u_x u_r}}{\dfrac{\partial \overline{U}_x}{\partial r}}; \quad \nu_{Tr\varphi} = \frac{-\overline{u_r u_r}}{\dfrac{\partial \overline{U}_\varphi}{\partial r} - \dfrac{\overline{U}_\varphi}{r}},$$

taking into account the directional character of the eddy-viscosity coefficient. The radial distributions of both these coefficients, corresponding to one value of $s = 0.31$ and presented in figures 28 and 30 for $x/D \geqslant 9$, exhibit an entirely different character. The ν_{Trx} coefficient is practically constant in lateral cross-sections of the jet and its value slightly increases in the region $9 < x/D < 15$. This tendency, illustrated more clearly in figure 29, does not exclude the constant ν_{Trx} value that may be attained at a sufficiently far distance from the nozzle in the region of fully self-preserving flow.

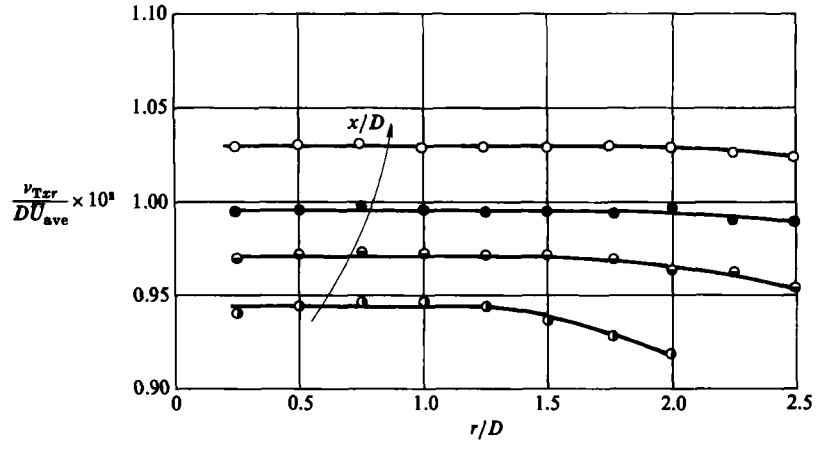

FIGURE 28. Normalized radial distributions of eddy-viscosity coefficient ν_{Txr} at $\overline{\Theta}_{ave} = 40°$ and $s = 0.31$: ◑, $x/D = 9$; ◒, 11; ●, 13; ○, 15.

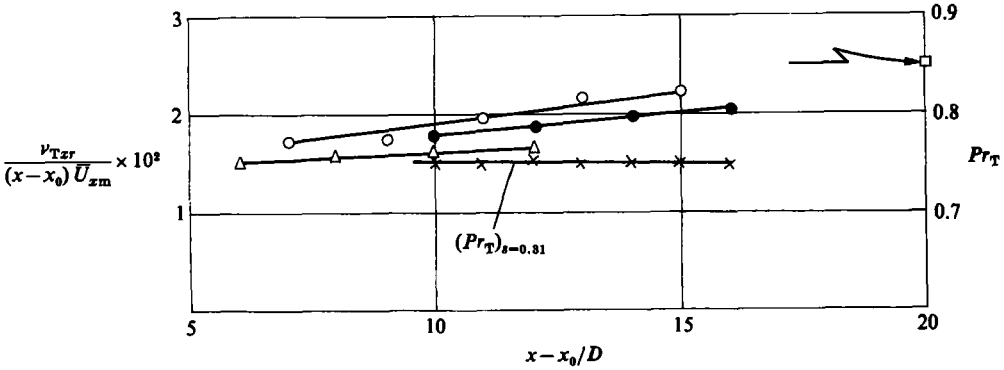

FIGURE 29. Downstream evolution of eddy-viscosity coefficient and turbulent Prandtl number in a fully developed turbulent flow at $\overline{\Theta}_{ave} = 40°$: ν_{Txr} – ○, $s = 0$; ●, 0.31; △, 0.42; □, after Komori & Ueda (1984) for $s = 0$, $(x-x_0)/D \geqslant 47$; and ×, Pr_T for $s = 0.31$.

Such a conclusion seems to be supported in figure 29 by the data of Komori & Ueda (1984), obtained, however, in a different flow configuration (non-swirling jet issuing into the ambient coflowing stream which has the velocity $\overline{U}_a = 0.072\overline{U}_{ave}$).

The distributions of the $\nu_{T\varphi}$ coefficient plotted in figure 30 exhibit a considerable radial non-homogeneity which increases in the downstream direction. However, when expressed in figure 31 in the form $\nu_{T\varphi}/(\nu_{T\varphi})_{max} = f(r/r^*)$, where r^* denotes the radial position of $(\nu_{T\varphi})_{max}$, all the experimental data tend to group fairly well and are in relatively close agreement with the rearranged results of Lilley & Chigier (1971).

The coefficient of turbulent heat diffusion a_{Tr} was also calculated, at the same cross-sections $x = \text{const.}$, from the relationship

$$a_{Tr} = \frac{-\overline{u_r \vartheta}}{\partial\overline{\Theta}/\partial r}$$

and plotted in figure 32 for $s = 0.31$. The ratio of coefficients a_{Tr} and ν_{Tx} determines the turbulent Prandtl number Pr_T which is kept constant at a level of 0.75 within the range $x/D = 9$–15 as seen in figure 29. This result corresponds well with the value of 0.71 measured by Komori & Ueda (1984).

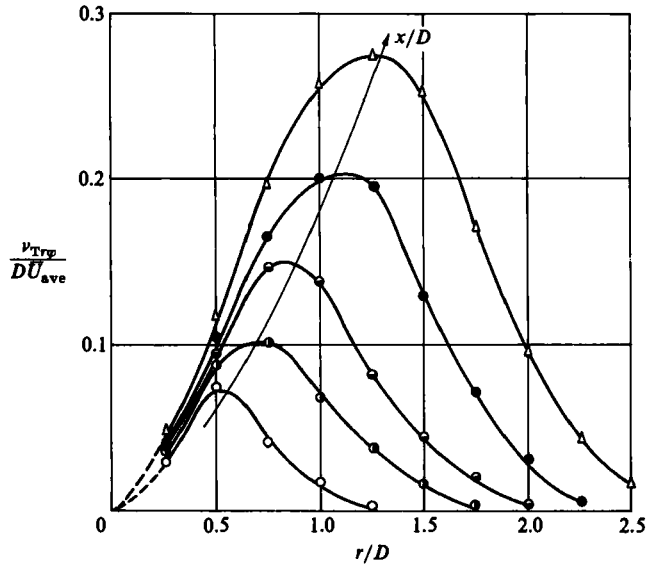

FIGURE 30. Normalized radial distributions of eddy-viscosity coefficient $\nu_{Tr\varphi}$ at $\bar{\theta}_{ave} = 40°$ and $s = 0.31$: ○, $x/D = 7$; ◑, 9; ◒, 11; ●, 13; △, 15.

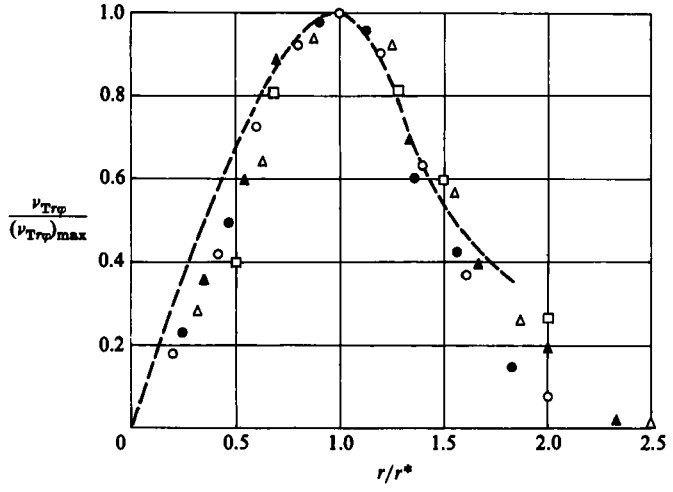

FIGURE 31. Universal form of $\nu_{Tr\varphi}$ profiles at $\bar{\theta}_{ave} = 40°$ and $s = 0.31$: ○, $x/D = 7$; ●, 9; △, 11; ▲, 13; □, 15; ———, after Lilley & Chigier (1971) for $s = 0.4$.

6. Concluding remarks

The experimental investigations of slightly heated swirling jets were carried out over the range of swirl degree s up to 0.42. The results obtained have proved the previous observation concerning the faster spread of a jet under swirl action. The measurements have also confirmed the validity of self-preservation of mean-flow quantities in the region beyond $x/D \approx 7$. However, this conclusion cannot be extended to the turbulence structure as the present measurements were not made far enough downstream to obtain self-preservation of turbulent motion.

The most interesting result of the present research, not previously stated, concerns

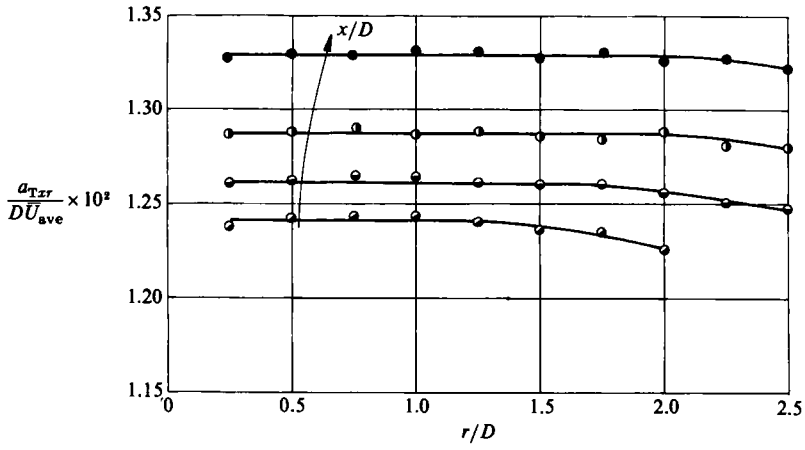

FIGURE 32. Normalized distributions of turbulent-heat-diffusion coefficient across the jet at $\bar{\theta}_{ave} = 40°$ and $s = 0.31$: ◑, $x/D = 9$; ◒, 11; ◑, 13; ●, 15.

the influence exerted by swirl on the downstream evolution of turbulent quantities. Experimental data have shown that in the near flow region the swirl action promotes the non-homogeneity of the mean-velocity field and creates a deformation bubble with a strong velocity gradient inside. In consequence, all the turbulent transport processes are also intensified, which causes considerable growth of the overall turbulence level. The intense turbulent mixing next leads to faster equalization of the mean flow and to the more intense decay of turbulent quantities further downstream.

It has also been stated that the eddy-viscosity coefficients ν_{Trx} and $\nu_{Tr\varphi}$ exhibit qualitatively different radial distributions and, within the range $x/D = 9$–15, their values increase in the downstream direction. In this region the turbulent Prandtl number remains constant, and for the medium swirl degree $s = 0.31$ its value has been estimated at about 0.71.

REFERENCES

ACHMEDOV, R. B. 1977 *Aerodinamika zakrucennoj strui*. Moscva: Energia.

ALLEN, R. A. 1970 Aerodynamics and interaction of single and multiple jets with rotation. Ph.D. thesis, University of Sheffield.

CHIGIER, N. A. & BEÉR, J. M. 1964 *Trans. ASME* D: *J. Basic Engng* **86**, 788.

CHIGIER, N. A. & CHERVINSKY, A. 1967 *Trans. ASME* E: *J. Appl. Mech.* **34**, 443.

CURTET, R. M. & DARIGOL, M. 1978 Aerothermique d'un jet libre tournant turbulent. Preprint, Institute de Mecanique, Grenoble.

ELSNER, J. W. & DROBNIAK, S. 1979 In *Transportprozesses in turbulenten Strömungen*. Berlin: Akademie der Wissenschaften der DDR.

ELSNER, J. W. & DROBNIAK, S. 1983 In *Structure of Complex Turbulent Shear Flow* (ed. R. Dumas & L. Fulachier). Springer.

ELSNER, J. W. & MUSIALIK, M. 1982 In *Turbulenzmodelle und ihre Anwendung in der Technik*. Berlin: Akademie der Wisenschaften der DDR.

GRANDMAISON, E. W. & BECKER, H. A. 1982 *Can. J. Chem. Engng* **60**, 76.

KERR, N. M. & FRASER, D. 1965 *J. Inst. Fuel* **38**, 519.

KOMORI, S. & UEDA, H. 1984 *Phys. Fluids* **27**, 77.

KOMORI, S. & UEDA, H. 1985 *Phys. Fluids* **28**, 2075.

KUBO, I. & GOULDIN, F. C. 1975 *Trans. ASME* I: *J. Fluids Engng* **97**, 310.

KURZAK, L. 1982 Turbulent heat diffusion in free axi-symmetric jet (in Polish). Ph.D. thesis, Technical University of Częstochowa.

LILLEY, D. G. & CHIGIER, N. A. 1971 *Intl J. Heat Mass Transfer* **14**, 573.

LOYTSYANSKII, L. G. 1953 *Prikl. Math. Mech.* **17**, 3.

OGAWA, A., HATAKAYAMA, H. & FUJITA, Y. 1979 *15th Rep., J. College Engng Nihon Univ.* A, p. 20.

OGAWA, A., HATAKAYAMA, H. & FUJITA, Y. 1981 *2nd Rep., J. College Engng Nihon Univ.* A, p. 22.

OGAWA, A., HATAKAYAMA, H. & FUJITA, Y. 1982 *3rd Rep., J. College Engng Nihon Univ.* A, p. 23.

PRATTE, B. D. & KEFFER, J. F. 1972 *Trans. ASME* D: *J. Basic Engng* **94**, 739.

ROSE, W. R. 1962 *Trans. ASME* E: *J. Appl. Mech.* **29**, 615.

TKACKAJA, O. S. & USTIMIENKO, B. P. 1971 *Problemy teploenergetiki i prikladnoj teplofiziki* **7**, 175.

TOWNSEND, A. A. 1956 *The Structure of Turbulent Shear Flow.* Cambridge University Press.

TRAUGOTT, S. C. 1958 *NACA TN* 4135.

WYGNANSKI, I. J. & FIEDLER, H. F. 1969 *J. Fluid Mech.* **38**, 577.